



Effect of Probe Lifting Height in Jumping Mode AFM for Living Cell Imaging

Can Cheng^{1,2,3} · Xingyue Wang^{1,2,3} · Jianjun Dong^{1,3} · Zuobin Wang^{1,2,3,4} 

Received: 31 January 2023 / Revised: 6 April 2023 / Accepted: 7 April 2023
© The Author(s) 2023

Abstract

Atomic force microscopy (AFM) is one of the effective methods for imaging the morphological and physical properties of living cells in a near-physiological environment. However, several problems caused by the adhesion of living cells and extension of the cell membranes seriously affect the image quality during living cell imaging, hindering the study of living cells. In this work, jumping mode AFM imaging was used to image living cells at varied probe lifting heights to meet image quality requirements, and image quality related to the probe lifting height is discussed in detail. The jumping mode was divided into three parts based on the varying heights of the lifted probe, namely near-contact mode, half-jumping mode, and full-jumping mode, and the causes of their imaging drawbacks were analyzed. At an appropriate lifting height, the probe can be completely free from the influence of cell adhesion and self-excited oscillation, thus avoiding the occurrence of “trail” phenomena and invalid points in the imaging of living cells and improving the image quality. Additionally, this work provides a new approach to calculating the lateral force through the adhesion of trace and retrace scanning at a low height, which is important for studying the extension characteristics of the cell membrane.

Highlights

- This paper systematically studies the effects of the jumping mode on imaging, which is helpful in obtaining accurate morphological information and shortening the imaging time.
- The causes of “trail” and invalid points in the jump mode were analyzed.
- A new method to calculate the vertical and lateral adhesion forces on cell surfaces for studying the extensibility of the cell membrane was proposed.

Keywords Atomic force microscopy · Jumping mode · Lifting height · Living cell imaging

✉ Zuobin Wang
wangz@cust.edu.cn

¹ International Research Centre for Nano Handling and Manufacturing of China, Changchun University of Science and Technology, Changchun 130022, China

² Centre for Opto/Bio-Nano Measurement and Manufacturing, Zhongshan Institute of Changchun University of Science and Technology, Zhongshan 528437, China

³ Ministry of Education Key Laboratory for Cross-Scale Micro and Nano Manufacturing, Changchun University of Science and Technology, Changchun 130022, China

⁴ JR3CN & IRAC, University of Bedfordshire, Luton LU1 3JU, UK

1 Introduction

The geometric and mechanical properties of living cells is considered to be a new field in biology and may make a considerable contribution to the study of human diseases [1, 2]. These important characteristics describe how cells sense, including their division, migration, shape, and interaction with the surrounding environment [3, 4]. Hence, studies of living cells are helpful in further understanding the pathophysiology and pathogenesis of human diseases [5, 6].

Since its invention, the atomic force microscope (AFM) has proven itself to be a standard tool of biological science. It can image biological samples with high resolution and detect molecular interactions between biological

molecules under near-physiological conditions [7–9]. With its ability to function in near-physiological conditions, AFM can help quantify the geometric and mechanical properties of living cells and use these properties to evaluate the effects of drug treatment or different types of pathologies [10, 11]. The shapes of eukaryotic cells and the organisms they ultimately form are determined by periodic mechanosensing, mechanotransduction, and mechanoresponse [12]; therefore, the cell morphology reflects the interaction among cytoskeletons, cell membrane, and cell–substrate adhesions [13]. Furthermore, cell morphological transformation has been proven to be the precursor and one of the important influences on gene expression and enzyme reactions [14]. Stiffness imaging and morphological imaging are helpful for understanding the behavior of living cells [15]. However, due to the particularities of biological samples (such as softness, complex morphology, and high adhesion), accurate imaging of living cells in a liquid environment close to the physiological state remains a challenge.

According to the force between the tip and sample during scanning, the working mode of AFM can be categorized into three types, namely contact mode, tapping mode, and intermittent contact mode. The contact mode has some well-known drawbacks, such as for samples with steep edges and those that are soft, sticky, or loosely attached to the surface [16, 17]. In the contact mode, the tip is always in contact with the sample during scanning. The direct vertical deflection of the cantilever is used as the feedback signal. An imaging setpoint is set, and the feedback adjusts the piezo height to keep this setpoint deflection constant. On the cell surface, where the cell height increases and decreases greatly, the difference between the setpoint and the measured value of the feedback is limited by the free state of the cantilever. Hence, the feedback responds slowly to the changes. This phenomenon leads to differences in the “UP” and “DOWN” regions of the tip scanning determined by comparing the trace and retrace of scans. When the feedback is not rapid enough for the scan speed and topographic change, the scan lines tend to “trail” as the tip follows the surface downward, making the imaging of cell shapes inaccurate. The shear force easily damages the soft sample when the probe moves laterally [18]. The most common modes, namely contact mode and traditional tapping mode, deal with undesired forces that might damage or compress the sample. In the tapping mode, the absolute vertical force cannot be controlled, leading to the compression of soft samples and complications on sticky samples [19]. Some other modes have been developed to overcome the above difficulties. For instance, the jumping mode is used to image the structure of complex biological systems and obtain the force–distance (FD) curve array of samples and map them pixel by pixel. This array is directly related to the shape of biological samples. Given that the

tip vertically jumps from one image point to another, the jumping mode is named as is [20, 21]. The tip moving algorithm can prevent the lateral force and control the vertical force, making straightforward nondestructive imaging. This mode can solve problems with soft materials, sticky samples, loosely attached samples, or samples with steep edges. Thus, the jumping mode can fully control the tip–sample force at each pixel of the image. However, the imaging time spent in this mode is longer than that in other modes. Reducing the distance of FD curves of each pixel can reduce the scanning time but may cause some problems in the image, such as “trail” phenomena and invalid points.

In this work, we defined the jumping mode in three forms, namely near-contact mode, half-jumping mode, and full-jumping mode, according to the contact height between the tip and the surface of the sample. In each form, the influence factors of the imaging of living cells were analyzed in detail. The causes of “trail” and invalid points in the jump mode were also determined. This study revealed that systematically understanding the effects of the jumping mode on imaging is helpful in obtaining accurate morphological information and shorten the imaging time. By examining the near-contact mode, we proposed a new method to calculate the vertical and lateral adhesion forces on cell surfaces for studying the extensibility of the cell membrane.

2 Materials and Methods

Living SMMC-7721 cells were cultured at 37 °C (5% CO₂) in a culture medium (RPMI-1640) containing 10% fetal bovine serum. All experiments were performed using an atomic force microscope (NanoWizard BioScience, JPK, Bruker, Germany). This device can obtain a complete FD curve at each pixel of the image and give complete information on the interactions of local tip samples with high spatial resolution. This feature is especially important for obtaining accurate adhesion data because of the dependence of the measured adhesion value on the velocity during the acquisition of an FD curve [22]. A simplified representation of the tip movement is shown in Fig. 1a and b. The separation distance between the tip and sample (*Z* length) can be set by users.

In the jumping mode, the *Z* piezo extends, moves the cantilever toward the surface until the setpoint is reached, and retracts it again. An FD curve is collected by each pixel of the image, as shown in Fig. 1c. The cantilever can bend due to changes in the environment, such as temperature, PH, and ionic strength in the liquid. Therefore, a baseline (the red line) was used to correct the vertical drift and measured at the beginning of each scan line. In a full force curve, the approaching and retracting parts usually differ; one of the reasons for this variation is the hydrodynamic resistance on

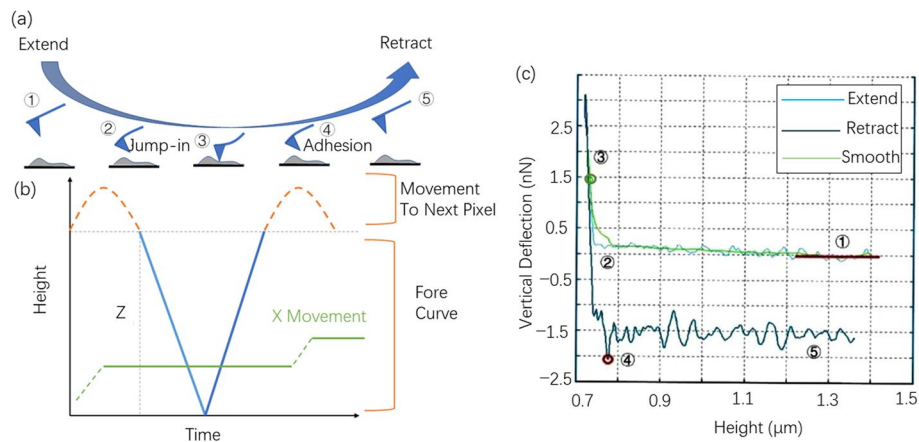


Fig. 1 Schematic view of the tip movements in the jumping mode and the FD curves. **a** Deformation of the cantilever while it extends and retracts from the surface of the sample. **b** Tip movement algorithm in the jumping mode; an FD curve is recorded in the absence of the XY movement of the tip. **c** FD curve recorded for each pixel; the numbers on the curve correspond to the marked status in (a); part ① on the extended line is used as the baseline, which can be used to correct

for changes in the vertical deflection of the cantilever over time. The *green curve* represents the smooth processing of the extended line, which is used to eliminate noise and facilitate mechanical calculation. The *green circle* represents that the tip reaches the setpoint during the extended process. The *red circle* represents the adhesion force when the tip leaves the sample

the cantilever in the liquid, which leads to a difference in the zero-force line [22, 23].

In the contact part of the force curve, the elastic and adhesive deformations of the cell are related to its Young's modulus, regardless of the approach or retraction stage. The elastic constant K of the sample can be calculated as follows:

$$K = 4E/3(1 - \nu^2), \quad (1)$$

where E is the Young's modulus, and ν is the Poisson's ratio of the sample. The relationship among force, indentation, and contact radius can be expressed by the Hertz model as follows:

$$\delta = a^2/R, \quad (2)$$

$$a = (F_n R/K)^{1/3}, \quad (3)$$

where δ is the indentation, a is the contact radius, R is the radius of the tip, and F_n is the applied normal force. The theory of adhesive contact mechanics was proposed by Johnson et al. (JKR theory) [24], who modified the classical Hertz theory to explain the effect of surface energy. Meanwhile, Refs.[25, 26] proposed another theory (DMT theory) that is suitable for the small contact area between the tip and the sample. In this study, the tip is a triangular pyramid with a small contact area, so the DMT theory was used. The Young's modulus was calculated by the DMT algorithm after the extended curve was analyzed. The adhesion force was calculated from the maximum force that occurs when the tip leaves the sample in the retract curve.

3 Results and Discussion

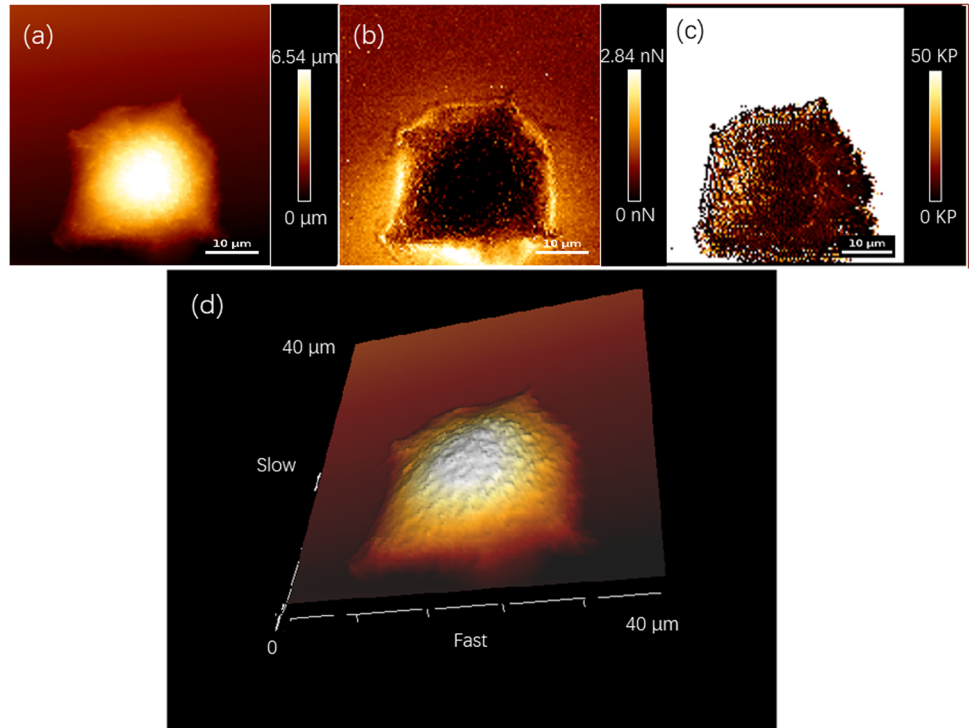
The SMMC-7721 cells were imaged with RPMI-1640. The cantilever used in the experiments was MLCT-Bio (0.07 N/m, Bruker). The SMMC-7721 cells were imaged under different conditions by changing the Z value. Three modes were adopted in the experiments.

3.1 Full-Jumping Mode ($Z \geq 1000$ nm)

In the full-jumping mode, no "trail" appeared throughout the different scanning tracks. Given that the tip is in vertical contact with the sample, the Z length is sufficient to completely separate the tip from the sample surface. The lateral force between the tip and the sample and the lateral deformation of the surface can be avoided. In addition, the "trail" caused by insufficient feedback can be avoided when the tip scans the surface downward because each pixel of the image depends on the complete FD curve.

With the movement, the extension of the tip can be used to describe the attraction, repulsion, or deformation of the sample. When the tip contracts, the interaction can be measured to describe the adhesion, elastic modulus, or energy dissipation of samples, as shown in Fig. 2. The SMMC-7721 cells are shaped as irregular circles with a diameter of about 30 μm and height of about 6 μm , as shown in Fig. 2a. As displayed in Fig. 2b, the adhesion of the cells at the edge is greater than that near the nucleus because of the high elasticity and height of the nucleus. As illustrated in Fig. 2c and d, the lifting height Z within this range can clearly and

Fig. 2 Height and quantitative maps of multiple properties of the cell with the Z length of 1500 nm. **a** Height and **b** adhesion maps of the cell. **c** Map of Young's modulus, which reflects the elasticity of the cell surface. **d** 3D map of the cell



accurately express the physical characteristics and morphology of the cell.

3.2 Half-jumping mode ($300 \text{ nm} < Z < 1000 \text{ nm}$)

When $300 \text{ nm} < Z < 1000 \text{ nm}$, the morphology of the cells is basically visible under different Z lengths. When the Z length decreases, the “trail” on the image becomes evident, as shown in Fig. 3. We then analyzed the reasons for the “trail” in the jumping mode by changing the scan angles to 0° and 180° to simulate the trace scanning and retrace scanning of the contact mode. As shown in Figs. 4b–c, the images scanned from different angles have the same “trail” positions (“DOWN” region, the red circles). The “trail” is caused by the difference between the jumping mode and

contact mode. The two curves in Figs. 4d and e represent the force curves of the “UP” and “DOWN” regions, respectively. Figure 4g reveals that when the tip separates from point A and moves to point B at the “UP” part, the length of the extended force curve (Z_B) is smaller than the set Z length (Z_s) because the height of B is larger than that of A. For the same reason, at the “DOWN” part, the length of the extended curve Z_D is larger than the set Z length ($Z_D > Z_s$) because the height of point D is smaller than that of C. On the basis of the measured height curve of the same cell at the full-jumping mode (the Z length and scan angle are 1000 nm and 0° , respectively), the curves of the “UP” and “DOWN” parts can be approximated in a straight line. Therefore, the slopes of the two parts can be calculated as follows:

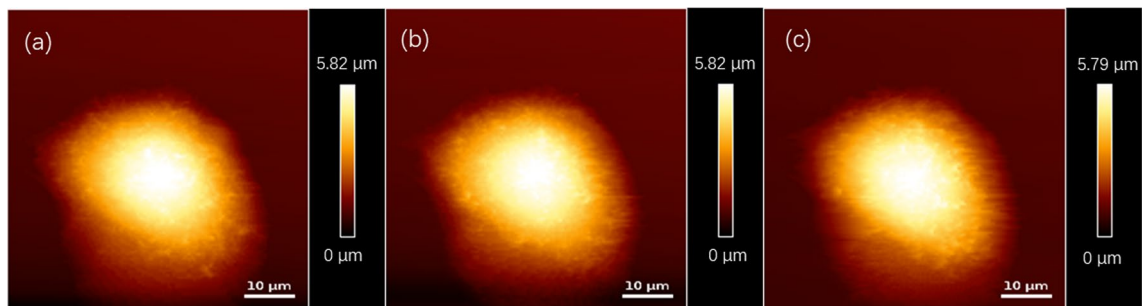


Fig. 3 Height images changed with the Z length. **a**, **b**, and **c** were imaged at 800, 600, and 400 nm, respectively. The morphologies of

cells are visible; when the Z length decreases, the “trail” becomes evident

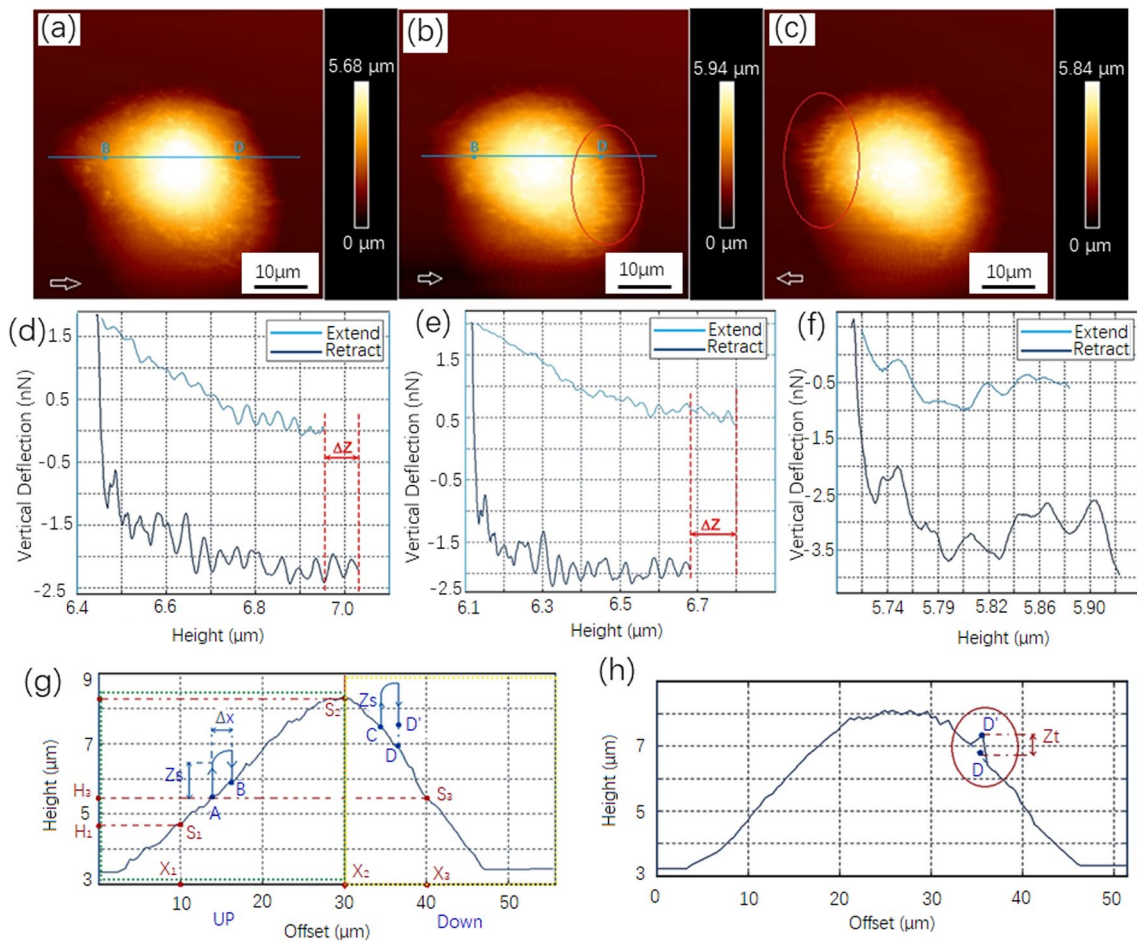


Fig. 4 **a** Height image with the Z length of 1000 nm. **b** and **c** are imaged at 500 nm, and the *white arrows* indicate the scanning direction, and the *red circles* show where the “trail” occurs. **d** and **e** are the force curves of points B and D in **(a)**, respectively. The value of ΔZ

in **d** is 0.083 μm , and the value of ΔZ in **e** is 0.118 μm . **f** is the force curve of point D in **(b)**. **g** and **h** are the heights of the cell at the *blue lines* in **(a)** and **(b)**, respectively

$$\begin{cases} K_u = (H_2 - H_1)/(X_2 - X_1) \approx 0.18 \\ K_d = (H_3 - H_2)/(X_3 - X_2) \approx -0.27 \end{cases} \quad (4)$$

Given that the size of the image is $60 \times 60 \mu\text{m}$ and the resolution is 128×128 , the length of each X movement is $\Delta x = 60 \mu\text{m}/128 \approx 469 \text{ nm}$. The higher the resolution, the smaller the Δx . With the slopes in Eq. (4), the height variation of each X movement on the sample can be calculated as

$$\begin{cases} \Delta H_u = K_u \times \Delta x \approx 84.4 \text{ nm} \\ \Delta H_d = K_d \times \Delta x \approx -126.6 \text{ nm} \end{cases} \quad (5)$$

This relationship can be seen from the error length between the extended curve and the retracted curve. The errors can be expressed as

$$\Delta Z = Z_r - Z_e \quad (6)$$

Here, Z_r is the length of the retracted curve, and Z_e is the length of the extended curve. When the tip is in the “UP” part, the value of ΔZ is similar to ΔH_u (Fig. 4d). When the tip is in the “DOWN” part, the value of ΔZ is similar to ΔH_d (Fig. 4e). In the “trail” area (the red circle in Fig. 4h) of the “DOWN” part, the length of the extended curve Z'_D at the point D' is less than Z_D at the point D . When the tip reaches D' , the set point is reached due to interference, making Z'_D smaller than Z_D . The error value between the measured height and the actual height is expressed as:

$$Z_t = |Z'_e - Z_e| \quad (7)$$

Figures 4g and h represent the morphology of the same line on the cell with Z length of 1000 and 500 nm, respectively. The height error of the two measurements is 206 nm, which is extremely close to $Z_t = 203 \text{ nm}$ calculated using Eq. (7). Therefore, the reason for the “trail”

occurrence is the inaccurate judgment of the tip on the setpoint. The Z length is not large enough to overcome the separation point caused by adhesion, as observed from the retracted curve of Fig. 4f. As a result, the initial amplitude of the extended curve of the next point changes dramatically, and the baseline becomes difficult to calculate. In the case of an inaccurate baseline, errors are obtained in the measurement of the set point and the calculation of height. This mode in such a condition is called the half-jumping mode.

3.3 Near-contact mode ($0 \text{ nm} < Z \leq 300 \text{ nm}$)

When the Z length is less than 300 nm, the tip does not have enough distance to separate from the sample and is nearly in contact with the sample during scanning. Therefore, we defined this mode as the near-contact mode. Figure 5 shows that with the decrease in Z length, the number of invalid points gradually increases in the imaging process and finally affects the photo quality. The height of the tip (Z length) cannot reach the changing height of the sample, i.e., $Z_s < \Delta H$, where ΔH is the height variation of the sample in each X

movement. When the tip reaches the next point of the pixel, the deformation of the cantilever directly reaches or exceeds the set point value, leading to insufficient or even a lack of data on the extended curve. To improve the imaging quality, we can increase the value of Z_s and decrease the value of ΔH . ΔH can be achieved by increasing the resolution (decrease the Δx).

In the near-contact mode, diverse morphologies similar to the trace and retrace scanning of the contact mode were observed when the same cell was imaged at different angles. Figure 6 shows that the morphology and adhesion differ for varying angles. A comparison of the adhesion and height of the same position in the two pictures reveals that the different parts of the sample have varying errors (Table 1). In Table 1, each point is the same position in the two images. Figure 6a displays the “trace” and the “UP” part of the cytoplasmic, and Fig. 6b shows the “retrace” and the “DOWN” part of the cytoplasmic. F_l and Z_v are the calculated lateral force and the vertical length, respectively, and the error is the absolute value. The errors of the cytoplasmic part are larger than those of the substrate and the nuclear parts. When the adhesion of the cell at the

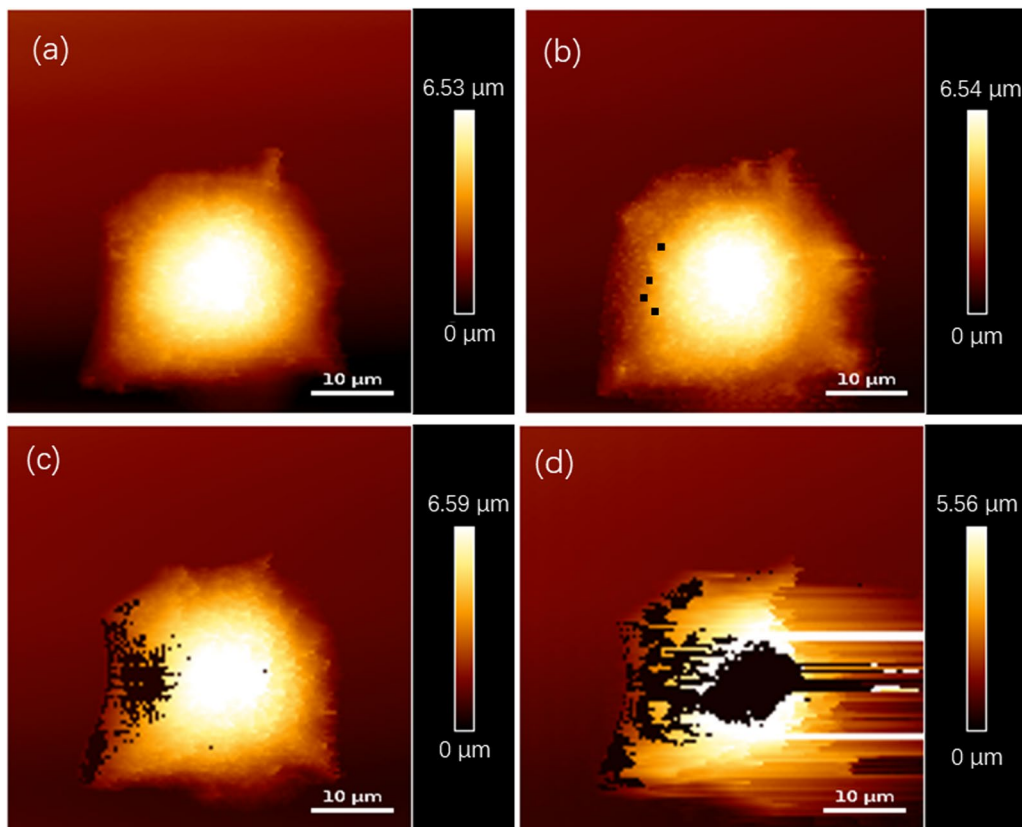


Fig. 5 Height images changed with the Z length. **a** is imaged at 1000 nm, and the cell is imaged clearly. **b** is imaged at 300 nm, the invalid points (*black points*) begin to appear. **c** is imaged at 200 nm, a

large number of invalid points (*black points*) appear at the “UP” part, and the cell morphology is basically visible. **d** is imaged at 100 nm, and the cell morphology cannot be identified

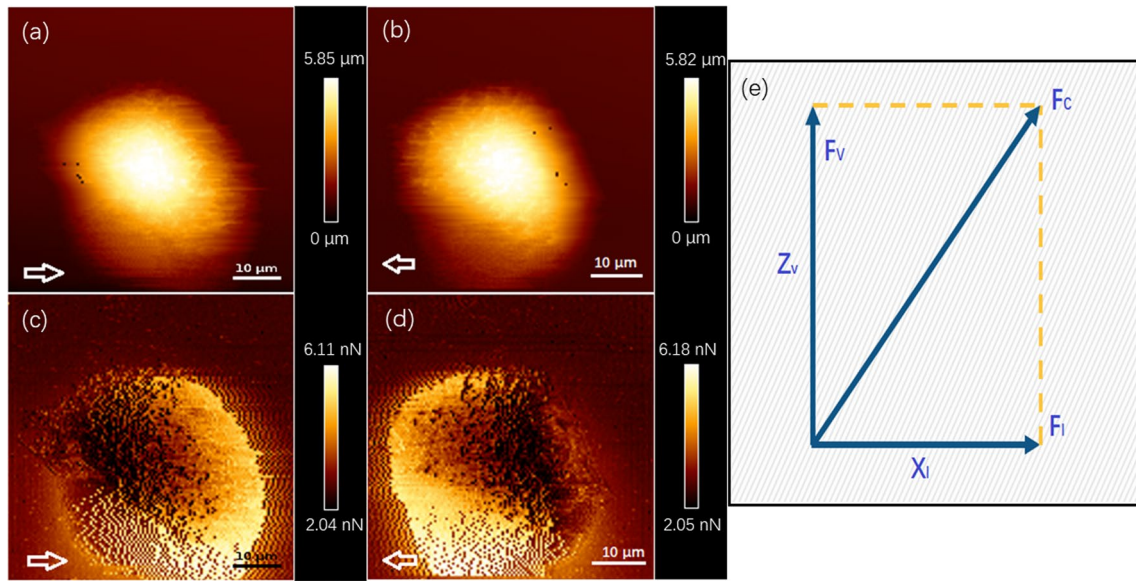


Fig. 6 **a, b** Height images with a Z length of 300 nm. **c** and **d** are the adhesion maps of the cell, and the *white arrows* indicate the scanning directions. **e** Schematic view of the decomposition of adhesion, where F_v is the adhesion in the vertical direction, F_l is the adhesion in the

lateral direction, F_c is the resultant force of F_v and F_l , Z_v is the deformation in the vertical direction, and X_l is the deformation in the lateral direction

Table 1 Examples of the points in the two images from Figs. 6a–b

Number	Area	Trace		Retrace		Error			
		Height (μm)	Adhesion (nN)	Height (μm)	Adhesion (nN)	Height (μm)	Adhesion (nN)	F_l (nN)	Z_v (μm)
1	Substrate	3.264	2.557	3.20	2.50	0.064	0.057	–	–
2		3.227	2.575	3.251	2.616	0.024	0.041	–	–
3		3.148	2.692	3.213	2.644	0.065	0.048	–	–
4	Nuclear	7.917	1.748	7.98	1.76	0.063	0.012	–	–
5		7.548	1.952	7.53	1.936	0.018	0.016	–	–
6	Cytoplasmic	3.102	3.018	3.486	4.621	0.384	1.603	3.499	0.404
7		3.019	2.86	3.4041	4.351	0.385	1.491	3.279	0.409
8		3.676	3.573	4.113	5.246	0.437	1.673	3.842	0.436
9		3.968	2.673	4.329	4.248	0.361	1.575	3.302	0.380
10		3.089	3.156	3.539	4.455	0.450	1.299	3.144	0.471

“UP” part was measured in the vertical direction, the tip moved similarly to the shape change of the sample. The adhesion of the cell at the “DOWN” part is a combination of vertical and horizontal forces. Therefore, the adhesions of the “UP” and “DOWN” parts at the same point can be obtained by scanning the same position at the opposite angle. The lateral adhesion force can be calculated via the mechanical decomposition shown in Fig. 6e, and the results are listed in Table 1.

Given that the tip is almost in contact with the sample during scanning, the above hypothesis was tested by examining the deformation of the cell surface. The lateral force F_l corresponds to the lateral deformation X_l ,

and $X_l = \Delta x = 469$ nm. According to the proper orthogonal decomposition, Z_v can be calculated as follows:

$$Z_v/X_l = F_v/F_l \tag{8}$$

The results are listed in Table 1. The obtained values of Z_v are almost equal to the absolute value of the errors between the two height measurements by different angles. This finding proves that the two scanning errors in different directions are obtained because the tip cannot detach from the adhesion force, leading to the extension of the cell membrane. Therefore, the correctness of the assumption that the lateral adhesion force can be obtained by

decomposing the adhesion force at the “DOWN” part has been proven.

4 Conclusions

In this work, the imaging effects of living cells at different heights in the jumping mode of AFM are compared, and the imaging quality at different heights is analyzed. The cause of the “trail” phenomenon and invalid points in living cell imaging is studied, and the Z length of the best image is determined by analyzing the mechanical changes of the probe in contact with the cell and combining these changes with the alterations in cell morphology. The optimal value of Z length avoids the influence of adhesion on the accuracy of probes and reduces the influence of too large Z value on the increase in cell imaging time, thus improving the accuracy and image quality of living cell imaging. Taking SMMC-7721 cells as an example, high-quality images of cell morphology can be obtained when the lifting height Z is higher than 1000 nm. However, the high lifting height of the tip can cause a long imaging time. When the lifting height Z is between 300 and 1000 nm, the imaging time is relatively short. Adhesion force has a small effect on the tip and causes errors in the image, such as the “trail” phenomenon, but does not affect the expression of the overall morphology of the cell. Therefore, the Z value at the critical point where the tip is completely free from the influence of cell adhesion can ensure the image quality and is the best choice for imaging time; that is, the size of Z is 1000 nm for SMMC-7721 cells. This principle can serve as a guide in finding the best image lifting height for different cells.

This work also provides a new method to calculate the lateral force through the adhesion of trace and retrace scanning at a low height. Through the comparison of height and adhesion between trace and retrace scanning, the point with skew force is decomposed vertically and horizontally. With these known vertical parameters of the point in the opposite direction, the lateral force in the horizontal direction can be obtained. This finding is helpful for the study of cell membrane extension characteristics in the future.

Acknowledgements This work was supported by National Key R&D Program of China (No. 2017YFE0112100), EU H2020 Program (MNR4SCCELL No. 734174), Jilin Provincial Science and Technology Program (Nos. 20180414002GH, 20180414081GH, 20180520203JH, and 20190702002GH), and “111” Project of China (D17017).

Author Contributions All authors read and approved the final manuscript.

Availability of Data and Material The authors declare that all data supporting the findings of this study are available within the article.

Declarations

Conflict of interest The authors declare that they have no conflicts of interest.

Open Access This article is licensed under a Creative Commons Attribution 4.0 International License, which permits use, sharing, adaptation, distribution and reproduction in any medium or format, as long as you give appropriate credit to the original author(s) and the source, provide a link to the Creative Commons licence, and indicate if changes were made. The images or other third party material in this article are included in the article's Creative Commons licence, unless indicated otherwise in a credit line to the material. If material is not included in the article's Creative Commons licence and your intended use is not permitted by statutory regulation or exceeds the permitted use, you will need to obtain permission directly from the copyright holder. To view a copy of this licence, visit <http://creativecommons.org/licenses/by/4.0/>.

References

1. Wu PH, Aroush DRB, Asnacios A, Chen WC, Dokukin ME, Doss BL, Durand-Smet P, Ekpenyong A, Guck J, Guz NV, Janmey PA, Lee JSH, Moore NM, Ott A, Poh YC, Ros R, Sander M, Sokolov I, Staunton JR, Wang N, Whyte G, Wirtz D (2018) A comparison of methods to assess cell mechanical properties. *Nat methods* 15(7):491–498
2. Benedetti M, Du Plessis A, Ritchie RO, Dallago M, Razavi SMJ, Berto F (2021) Architected cellular materials: a review on their mechanical properties towards fatigue-tolerant design and fabrication. *Mater Sci Eng R Rep* 144:100606
3. Struckmeier J, Wahl R, Leuschner M, Nunes J, Janovjak H, Geisler U, Hofmann G, Jähnke T, Müller DJ (2008) Fully automated single-molecule force spectroscopy for screening applications. *Nanotechnology* 19(38):384020
4. Wang Z, Lang B, Qu Y, Li L, Song Z, Wang Z (2019) Single-cell patterning technology for biological applications. *Biomicrofluidics* 13(6):061502
5. Leung K, Chakraborty K, Saminathan A, Krishnan Y (2019) A DNA nanomachine chemically resolves lysosomes in live cells. *Nat Nanotechnol* 14(2):176–183
6. Cross SE, Jin YS, Rao J, Gimzewski JK (2020) Nanomechanical analysis of cells from cancer patients. In: Balogh LP (ed) *Nano-enabled medical applications*. Jenny Stanford Publishing, pp 547–566
7. Zhou AH, McEwen GD, Wu YZ (2010) Combined AFM/Raman microspectroscopy for characterization of living cells in near physiological conditions. *Microsc Sci Technol Appl Educ*, 1.
8. Fotiadis D (2012) Atomic force microscopy for the study of membrane proteins. *Curr Opin Biotechnol* 23(4):510–515
9. Deng X, Xiong F, Li X, Xiang B, Li Z, Wu X, Guo C, Li X, Li Y, Li G, Xiong W, Zeng Z (2018) Application of atomic force microscopy in cancer research. *J Nanobiotechnology* 16(1):102
10. Zhu J, Tian Y, Wang Z, Wang Y, Zhang W, Qu K, Weng Z, Liu X (2021) Investigation of the mechanical effects of targeted drugs on cancerous cells based on atomic force microscopy. *Anal Methods* 13(28):3136–3146
11. Callies C, Schön P, Liashkovich I, Stock C, Kusche-Vihrog K, Fels J, Sträter A, Oberleithner H (2009) Simultaneous mechanical stiffness and electrical potential measurements of living vascular endothelial cells using combined atomic force and epifluorescence microscopy. *Nanotechnology* 20(17):175104

12. Vogel V, Sheetz M (2006) Local force and geometry sensing regulate cell functions. *Nat Rev Mol Cell Bio* 7(4):265–275
13. Keren K, Pincus Z, Allen GM, Barnhart EL, Marriott G, Mogilner A, Theriot JA (2008) Mechanism of shape determination in motile cells. *Nature* 453(7194):475–480
14. D'Anselmi F, Valerio M, Cucina A, Galli L, Proietti S, Dinicola S, Pasqualato A, Manetti C, Ricci G, Giuliani A, Bizzarri M (2011) Metabolism and cell shape in cancer: a fractal analysis. *Int J Biochem Cell B* 43(7):1052–1058
15. Liu Y, Li L, Chen X, Wang Y, Liu MN, Yan J, Cao L, Wang L, Wang ZB (2019) Atomic force acoustic microscopy reveals the influence of substrate stiffness and topography on cell behavior. *Beilstein J Nanotechnol* 10(1):2329–2337
16. Braet F, Wisse E (2004) Imaging surface and submembranous structures in living cells with the atomic force microscope. In *Atomic Force Microscopy*. Humana Press. 201–216
17. Gadegaard N (2006) Atomic force microscopy in biology: technology and techniques. *Biotech Histochem* 81(2–3):87–97
18. Brunner R, Simon A, Stifter T, Marti O (2000) Modulated shear-force distance control in near-field scanning optical microscopy. *Rev Sci Instrum* 71(3):1466–1471
19. Kasas S, Thomson NH, Smith BL, Hansma PK, Miklossy J, Hansma HG (1997) Biological applications of the AFM: from single molecules to organs. *Int J Imaging Syst Tech* 8(2):151–161
20. De Pablo PJ, Colchero J, Gomez-Herrero J, Baro AM (1998) Jumping mode scanning force microscopy. *Appl Phys Lett* 73(22):3300–3302
21. Dufrêne YF, Martínez-Martín D, Medalsy I, Alsteens D, Müller DJ (2013) Multiparametric imaging of biological systems by force-distance curve-based AFM. *Nat Methods* 10(9):847–854
22. Butt HJ, Cappella B, Kappl M (2005) Force measurements with the atomic force microscope: technique, interpretation and applications. *Surf Sci Rep* 59(1–6):1–152
23. Vinogradova OI, Butt HJ, Yakubov GE, Feuillebois F (2001) Dynamic effects on force measurements. I. Viscous drag on the atomic force microscope cantilever. *Rev Sci Instrum* 72(5):2330–2339
24. Johnson KL, Kendall K, Roberts A (1971) Surface energy and the contact of elastic solids. *Proceedings of the Royal Society of London. A. Mathematical and Physical Sciences* 324(1558):301–313
25. Prokopovich P, Perni S (2010) Multiasperity contact adhesion model for universal asperity height and radius of curvature distributions. *Langmuir* 26(22):17028–17036
26. Derjaguin BV, Muller VM, Toporov YP (1975) Effect of contact deformations on the adhesion of particles. *J Coll Interf Sci* 53(2):314–326

Publisher's note Springer Nature remains neutral with regard to jurisdictional claims in published maps and institutional affiliations.



Xingyue Wang She is currently a PhD student in Changchun University of Science and Technology. Her current research interest is micro- and nano-electronic technology.



Jianjun Dong He is currently a PhD student in Changchun University of Science and Technology. His current research interest is micro- and nano-electronic technology.



Zuobin Wang received his PhD from the University of Warwick (UK) in 1997. He is Professor and Director of International Research Centre for Nano Handling and Manufacturing of China, Changchun University of Science and Technology. His research interests are in the areas of nano-measurement, manipulation and manufacturing.



Can Cheng He is currently a PhD student in Changchun University of Science and Technology. His research interest is nano-measurement and manufacturing.